A Connection Between Star Formation Rate and Dark Matter Halos at $Z \sim 6$ In 2013 Planck Cosmology.

Felipe L. Gómez-Cortés[1]

Departamento de Física, Universidad de los Andes, Colombia

ABSTRACT

This work relates baryonic matter and dark matter at redshift $z = 5.9$ using observational data from CFHTLS (Willott et al. 2013), HST Legacy Survey (Bouwens et al. 2014; Finkelstein et al. 2014), UKIDSS and SDXS (McLure et al. 2009), and results of the Multidark Simulation (Klypin et al. 2014) in a cubic box of 1000Mpc h^{-1} length with 2013 Planck Cosmology (Planck Collaboration et al 2014). The Luminosity Function (LF) is fitted via four parameters with the Markov Chain Monte Carlo method. The relationship between the Dark Matter Halos Mass and Star Formation Rate is obtained using the relationship between the UV continuum (from the fitted LF) and Star Formation Rate (SFR) by Kennicutt (1998).Cosmic variance effects are studied on smaller boxes of 250Mpc h^{-1} length.

Subject headings: Dark Matter, UV Luminosity Function, Star Formation Rate, High Redshift Galaxies, Reionization

1. Observations

This paper is based on four main observational data sets from the Hubble Space Telescope and three ground-based telescopes. All $z \sim 6$ LBG candidates where discovered using using the drop-out technique(Steidel et al. 2003). All magnitudes are in AB system.

The data from the Hubble Space Telescope Legacy (HSTL) (Bouwens et al. 2014) is a compilation of observations since the installation of the Advanced Camera for Surveys (ACS) in 2002, through the near-infrared Wide Field Camera 3 (WFC3/IR) installed in 2009, up to 2012. The HST fields of view are: XDF, HUDF09-1, HUDF09-2, CANDELS-S/Deep, CANDELS-S/Wide, ERS, CANDELS-N/Deep, CANDELS-N/Wide, CANDELS-UDS, CANDELS-COSMOS and CANDELS-EGS, with areas of 4.7, 4.7, 4.7, 64.5, 34.2, 40.5, 62.9, 60.9, 151.2, 151.9 and 150.7 arcmin^2 respectively. The total area at redshift 6 corresponds to 740.8 arcmin^2 over five different lines of sight, wit a total volume of $1.8 \times 10^6 \mathrm{Mpc}^3$. Two cameras performed the observations: ACS and WFC3/IR, using B_{435}, V_{606}, i_{814}, z_{850}, I_{814}, Y_{098}, Y_{105}, $J125$, JH_{140} and H_{160} filters. The limit magnitude is between $\sim 27.5 \mathrm{mag}$ in CANDELS-EGS and$\sim 30 \mathrm{mag}$ in the deepest field (XDF). Total number of z=6 LBG candidates is 940, most of them in the faint end of the LF, magnitudes in the rest frame are in the range $-22.52 \leq M_{1600} \leq -16.77$ Bouwens et al. (2014) calculated LF using a stepwise maximum-likelihood (SWML) based on Efstathiou et al. (1988). The Schechter parameters derived are: $\phi^* = (0.33^{+0.15}_{-0.10}) \times 10^{-3} \mathrm{Mpc}^{-3}$, $M^*_{1600} = -21.16 \pm 0.20$ and $\alpha = -1.91 \pm 0.09$. Bouwens et al. (2014) reported that using just few fields of view, UVLF has a slightly non-Schechter-like form.

Finkelstein et al. (2014) worked also with HST, using the HUDF, CANDELS and GOODS fields, along with two of the Hubble Frontier Fields (HFF): deep parallel observations (unlensed fields) near the Abell 2744 and MACS J0416.1-2403 clusters. The HFF uses the ACS and the WFC3/IR with the same filters aforementioned but z_{850}. Total

survey area is around $\sim 300 \text{arcmin}^2$, with 706 photometric candidates at redshift 6 defined as the interval $5.5 < z < 6.5$. Total volume of this study is around $8 \times 10^5 \text{Mpc}^3$. The Schechter function parameters they found are $\phi^* = (1.86^{+0.94}_{-0.80}) \times 10^{-4} \text{Mpc}^{-3}$, $M^*_{1600} = -21.1^{+0.25}_{-0.31}$ and $\alpha = -2.02^{+0.10}_{-0.10}$.

Willott et al. (2013) presented the sixth release of the Canada-France-Hawaii Telescope Legacy Survey CFHTLS. The observations where performed over four separated fields covering a total area $\sim 4 \deg^2$ (a large area), it gives this survey great robustness. Optical observations used MegaCam with $u^* g' r' i' z'$ filters. The main selection criteria: all the objects must be brighter than magnitude $z' = 25.3$. The final number of LBGs founded was 40. Moreover, they get spectroscopic confirmation for 7 candidates using GMOS spectrograph on the Gemini Telescopes, which has a $\ll 5.5$-square arcmin field of view, giving a volume $\sim 1.09 \times 10^7 \text{Mpc}^3$. They show incompleteness in the sample due to foreground contamination and the detection algorithm; there is no warranty to have every object brighter than the limit magnitude on the faint limit. The full galaxy LF at $z = 6$ cannot be obtained as in other studies. Nevertheless, this survey was focussed on the highly luminous LBGs. LF is calculated using the stepwise maximum likelihood method of Efstathiou et al. (1988), within magnitudes from $M_{1350} = -22.5$ up to -20.5. The luminosity function of $z = 5.9$ shows an exponential decline at the bright end, where feedback processes and inefficient last cooling limites star forming in bright galaxies hosted in the most massive halos.

McLure et al. (2009) build the luminosity function for $z = 5$ and $z = 6$ using data from two ground-based telescopes: the United Kingdom Infrared Telescope in the near-IR imaging and Subaru Telescope for the optical imaging. They use the first data release of the UKIRT Infrared DeepSky Survey Ultra Deep Survey (UDS), together with the Subaru XMM-Newton Survey (SXDS). Total observed area is $0.63 \deg^2$ uniformly covered by booth

catalogues. The volume in this survey is $\sim 3 \times 10^6 \mathrm{Mpc}^3$. The UKIRT was equipped with the WFCAM using JK filters. The Subaru was equipped with the Suprime-Cam with the $BVRi'z'$ filters. All candidates where brighter than $z' = 26$. The UV rest frame magnitude range is $-22.4 \leq M_{1500} \leq -20.6$. The LF was calculated using the maximum likelihood estimator of Schmidt (1968). Their analysis gave a total number of 104 LBG candidates in the redshift range $5.7 \leq z \leq 6.3$. LF was parameterized according to the Schechter function with $\phi^* = (1.8 \pm 0.5) \times 10^{-3} \mathrm{Mpc}^{-3}$, $M_{1500}^* = -20.04 \pm 0.12$ and $\alpha = -1.71 \pm 0.11$.

The dataset was retrieved from McLure et al. (2009) graph using GAVO-DEXTER[1].
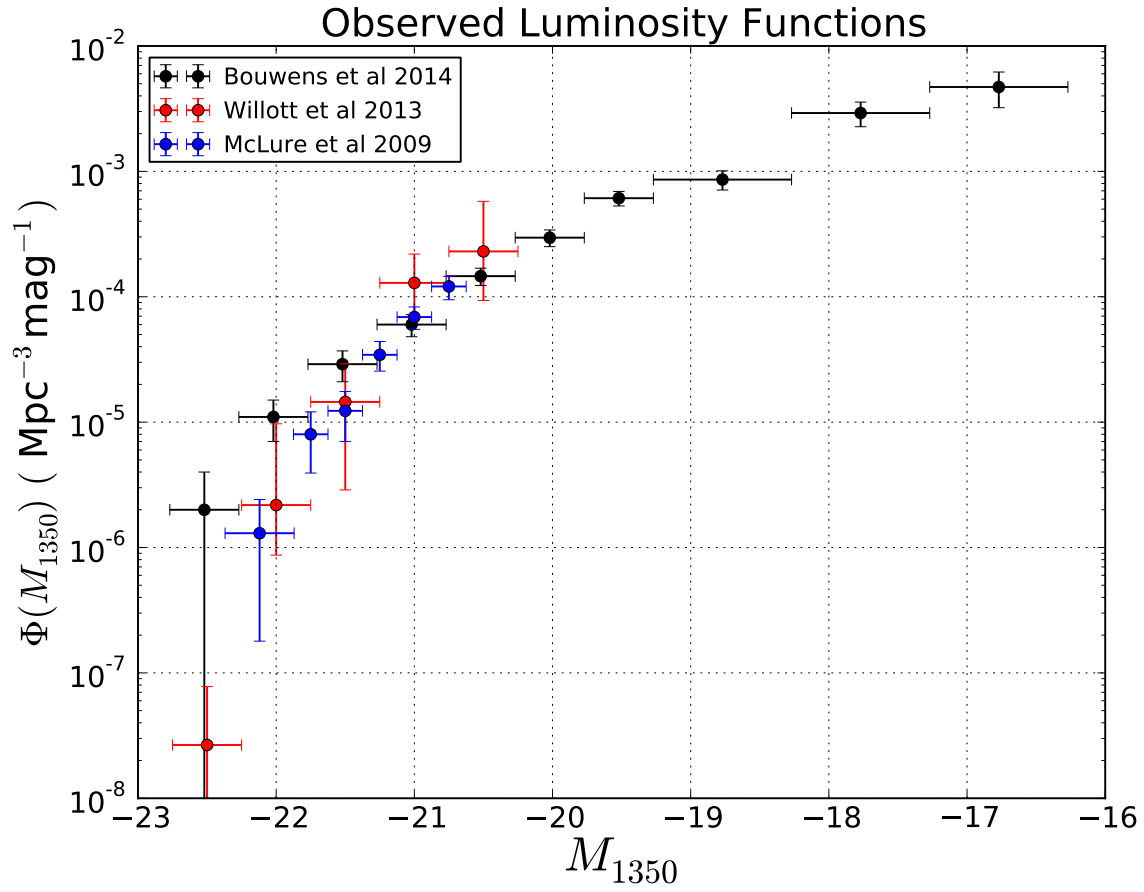
---

[1]http://dc.zah.uni-heidelberg.de/dexter/ui/ui/custom

Fig. 1.— Observational data from Bouwens et al. (2014); McLure et al. (2009)and Willott et al. (2013).

2. Methodology

The key element to connect SFR with halo mass from simulations is the observed UVLF. If there exist a function whom gives to each halo a UV luminosity then is posible to reproduce UVLF from DMH catalogs. The fitting parameters can be explored using a Markov Chain Monte-Carlo (MCMC) implementation. Once the parameters are found, the SFR-Halo Mass relation have been found.

We use the dark matter halo catalog from the Big MultiDark Plank 1 (MDPL) Simulation (Klypin et al. 2014) with 2013 Planck cosmology (Planck Collaboration et al 2014). MDPL is quite similar to the Big Bolshoi (1Gpc h^{-1}) (Prada et al. 2012) and its predecesor Bolshoi (Klypin et al. 2011) (250Mpc h^{-1}), booth of them with WMAP5 cosmology, but MDPL has bigger mass resolution. Those halo catalogs are available at the MultiDark Database[2] (Riebe et al. 2013).

The MDPL run is a N-body dark matter only simulation based on the L-Gadget2 code. The simulated volume is a cubic box of 1Gpc h^{-1} side length. It has 3840^3 dark matter particles of $1.51 \times 9 M_\odot h^{-1}$ mass each one. The 2013 Planck cosmology is defined by the following parameters: $\Omega_M = 0.307$, $\Omega_B = 0.048$, $\Omega_\Lambda = 0.730$, $\sigma_8 = 0.829$, $n_s = 0.96$ and $H_0 = 67.8$. The DMH Catalog at $z = 6$ contains $\sim 10.9 \times 10^7$ halos, to avoid incompleteness in the low mass end, halos with mass below $10^{10.3} M_\odot h^{-1}$ are rejected. In order to study how cosmic variance can affect measurements, the original catalog is divided into 64 small cubic boxes, with a similar volume to the observations.

The following treatment is applied to every one small box.

The halo abundance matching technique has been widely used (Colín et al. 1999; Kravtsov et al. 2004) resulting in good reproduction of the observed galaxy clustering.

---

[2]http://www.multidark.org

(Conroy et al. 2006; Lee et al. 2009). Here we use the simplest case with few premises:

1. Each halo in the catalog hosts one galaxy. There are not empty halos, also none of halos has two or more galaxies.

2. The UV luminosity of each galaxy is function of one variable; the mass of the DMH in which is located. This function must be monotone, this guarantees that most massive halos will host the most luminous galaxies in the same volume.

2.1. Fitting Model

The observed UV Luminosity Function has two slopes. To reproduce it we decide to use the four parameter model:

$$L_{\mathrm{UV}}(M) = L_0 M \left[\left(\frac{M}{M_0} \right)^{-\beta} + \left(\frac{M}{M_0} \right)^{\gamma} \right]^{-1} \tag{1}$$

where M is the hosting DMH mass, L_0 is a normalization constant, M_0 is the critical mass where the luminosity function has a slope change, β and γ are the slopes. This equation has a similar fashion to the mass to light relation (van den Bosch et al. 203) and the mean relation between stellar mas of a galaxy and the mass of its halo used by Moster et al. (2010).

2.2. Dust Attenuation

Dust in star forming galaxies absorbs part of the UV radiation and reemits on IR. The more massive is the galaxy then more dust contains and dust attenuation will be greater. The relation between dust attenuation and magnitude have been already studied, with this relation we can infer the dust-free UV luminosity of a galaxy from observations, resulting in a more accurate inferred SFR.

The UV Spectral Slope β was introduced by Meurer et al. (1999) as a UV color to study dust attenuation in local starburst galaxies and extrapolating to high redshift galaxies. This index appears when a power law fitting is performed over the spectral flux f as function of the wavelength λ;

$$f \propto \lambda^{\beta}.$$

The relation for ultra-violet attenuation at 1600Å they found is:

$$A_{1600} = 4.43 + 1.99\beta, \tag{2}$$

with A_{1600} in magnitude units.

Due LBGs have more similar spectra properties to local starburst galaxies rather than AGNs for example, we can assume that local calibration of $\beta - A_{1600}$ can be applied also for LBGs, "The main requirement is that the data include fluxes in two broad bands or coarse spectra covering the rest-frame UV."

Bouwens et al. (2012b) uses the fluxes on different bands to estimate β on each LBG candidate found with $z \sim 4 - 7$. After in redshift groups they found a linear relation between β and the UV magnitude:

$$\langle \beta \rangle = \frac{d\beta}{dM_{UV}} \left(M_{UV,AB} + 19.5 \right) + \beta_{M_{UV}=-19.5} \tag{3}$$

with $\beta_{M_{UV}=-19.5} = -2.20$ and $d\beta/dM_{UV} = -0.21$ at $z = 5.9$.

Smit et al. (2012) used the aforementioned relations to infer the corrected luminosity functions, i.e. dust-free luminosity functions, and the corrected SFR at $z = 4$.

Here we use the inverse relation, starting from the intrinsic or dust-free galaxy magnitude, obtaining the observed magnitude:

$$M_{obs} = \begin{cases} \frac{M_{int} - 4.616}{1.259}, & \text{if } A > 0 \\ M_{int}, & \text{else} \end{cases}. \tag{4}$$

2.3. MCMC

We used a Markov Chain Monte Carlo method to find the best parameters and its uncertainties over each one of the boxes and each observational dataset. The code was written on Python using the Scipy, Numpy and Matplotlib libraries.

First of all, one of the four observational data sets (Bouwens, Finkelstein, Willow and McLure) is selected to be the model to fit. From the whole simulated halo catalog, a subsample with cubic box shape of 250Mpc h^{-1} length is selected.

With an initial set of parameters (α, γ, M_0, and L_0) the UV luminosity for the halo is calculated as function of his mass according to equation 1. Then Luminosity is converted to magnitude units using:

$$M_{UV} = 51.82 - 2.5 \log_{10}(L_{UV}).$$

If we consider the dust attenuation im the equation 4 we have a dust-corrected UV Luminosity Function.

The luminosity function is constructed as an histogram of the magnitudes normalized by the volume of the catalog. Each observed luminosity function has a different bin range.

Once having the LF, we compare our LF against observed LF. The error function we consider is the sum of the square difference over each bin, divided by the observational data uncertain.

$$\chi^2 = \sum_{i=o}^{n} \frac{\left(x_{i,obs} - x_{i,fit}\right)^2}{2\sigma_i^2}$$

We worked on the logarithmic space of luminosities to have a good fitting on six decades.

The likelihood will have this property:

$$\mathcal{L} \propto \exp\left(-\frac{\chi^2}{n}\right)$$

, where n is the number of degrees of freedom. We have the maximum likelihood when the error is the minimum.

Each MCMC step will have have a small variation of the parameters, the UV luminosity and magnitude are calculated again for each halo, we have a new error χ^2_{new} and a new likelihood $\mathcal{L}_{new}$.

Following the Metropolis method, we compare the new and the old likelihood:

$$R = \frac{\mathcal{L}_{new}}{\mathcal{L}_{old}} = exp(\chi^2_{new} - \chi^2_{old})$$

If $R \geq 1$, then we immediate accept the new set of parameters and start the next MCMC step.

Else, we have a chance to keep the new set. When $R < 1$, we compare with a uniformly random number p in the range $[0, 1]$. if $R > p$ we accept the new set of parameters and start the next MCMC step. Else we reject the new set and start again with the old set.

We performed 10.000 effective MCMC steps, plus 1.000 thermalization steps over each box. We repeated for the same box without consider dust attenuation.

Then we perform the same method over the 64 boxes and the resting three data sets.

The restrictions imposed over the parameters where $0 \leq \alpha \leq 2.0$ and $\gamma \geq 0$.

Finally, the UV luminosity for each galaxy can be directly related with SFR according to Madau et al. (1998). This model is accurate within the range of $10^8 - 10^9 \mathrm{yr}$(Kennicutt 1998). The relation between UV luminosity and Star Formation Rate (Madau et al. 1998; Kennicutt 1998) is given by:

$$\mathrm{SFR}\left(M_{\odot}\mathrm{yr}^{-1}\right) = 1.4 \times 10^{-28} L_\nu \left(\mathrm{erg\ s}^{-1}\mathrm{Hz}^{-1}\right) \tag{5}$$

3.   Results

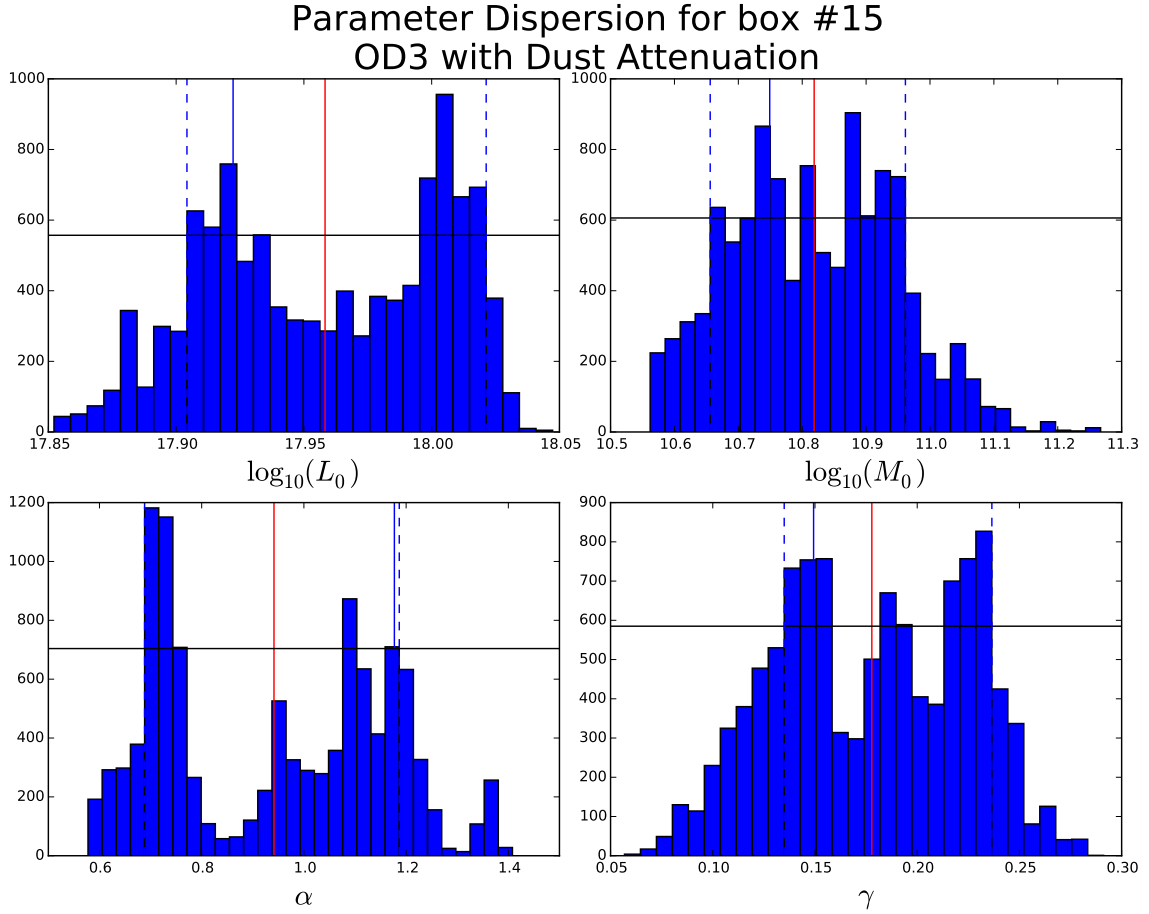γ always has the best coincidence for the minimum at the 10%.

Fig. 2.— Parameter dispersion: The 10.000 MCMC step parameters histogram for OD3 over the small boxe 15 with dust attenuation.
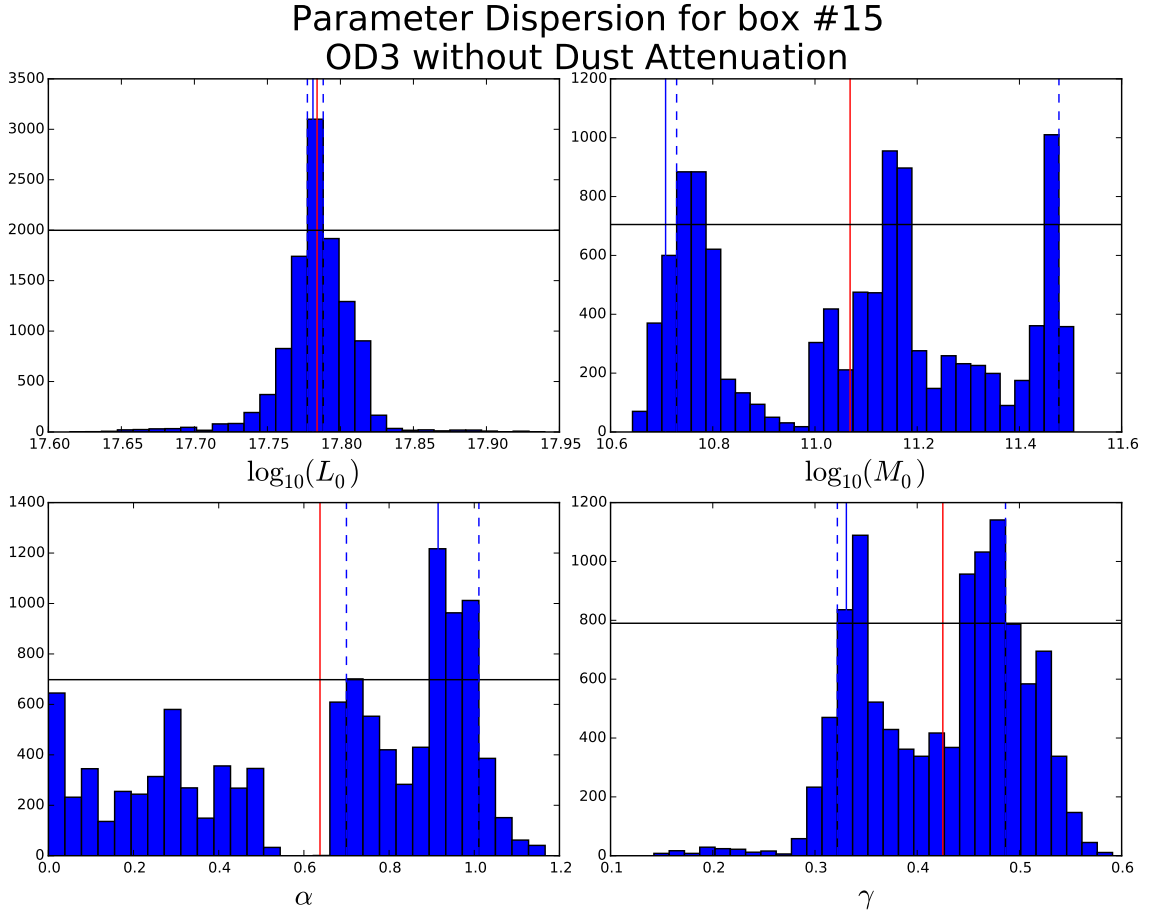
Fig. 3.— Parameter dispersion: The 10.000 MCMC step parameters histogram for OD3 over the small boxe 15 with dust attenuation.
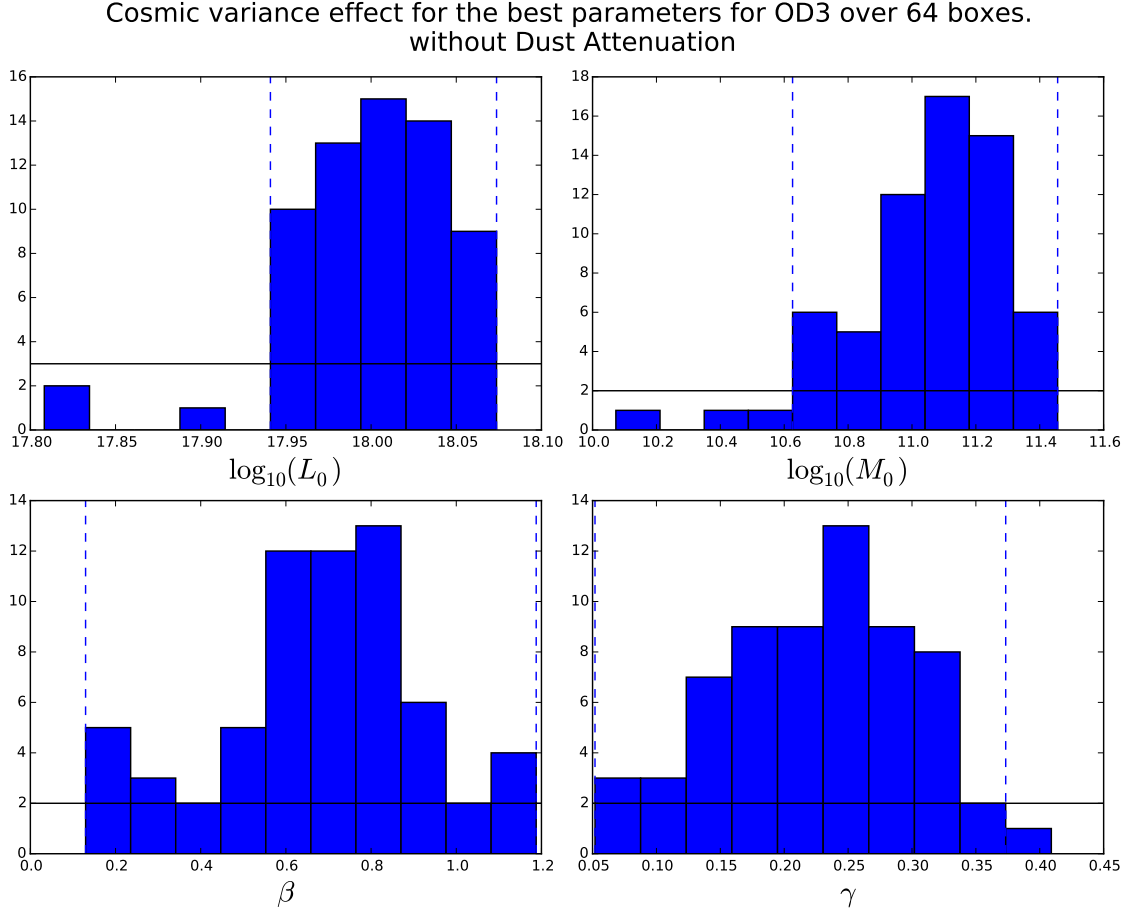
Fig. 4.— Cosmic Variance: The best fit parameters histogram for OD3 over the 64 small boxes with dust attenuation.
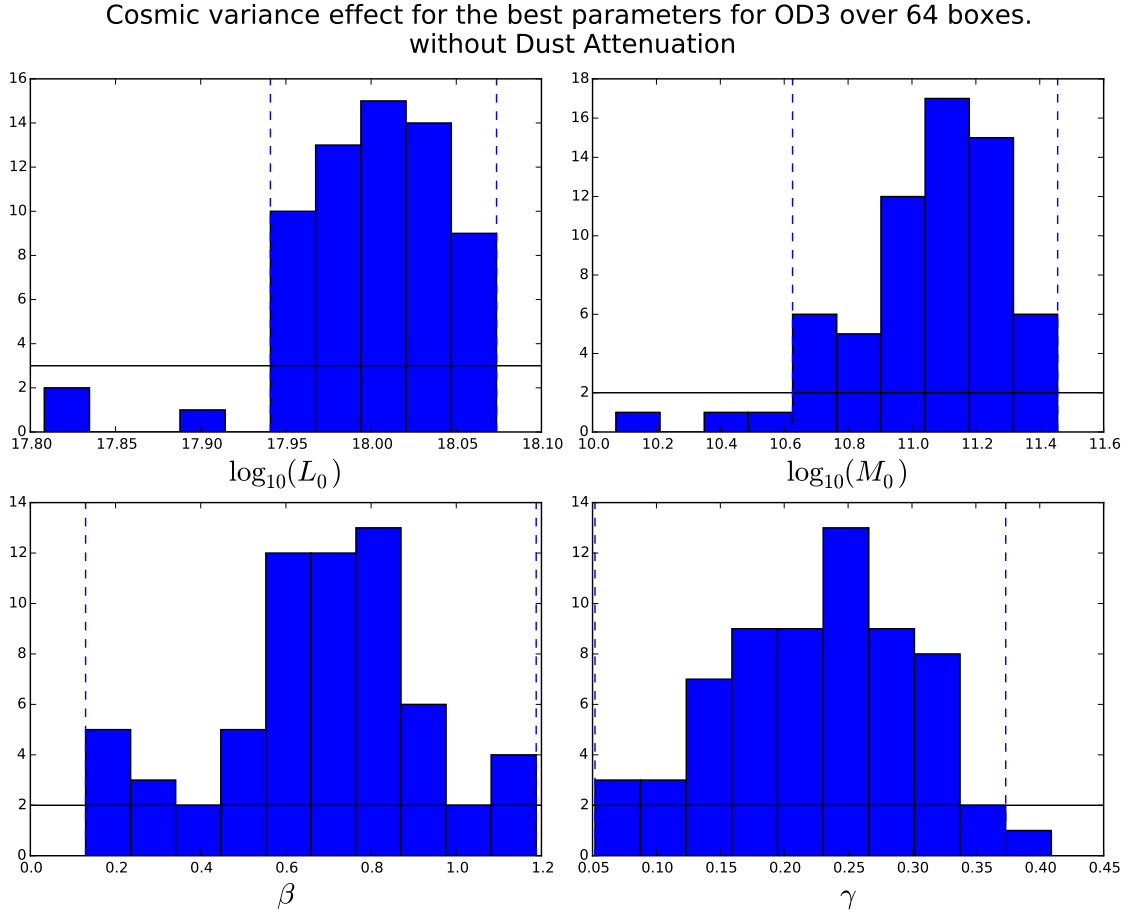
Fig. 5.— Cosmic Variance: The best fit parameters histogram for OD3 over the 64 small boxes without dust attenuation.
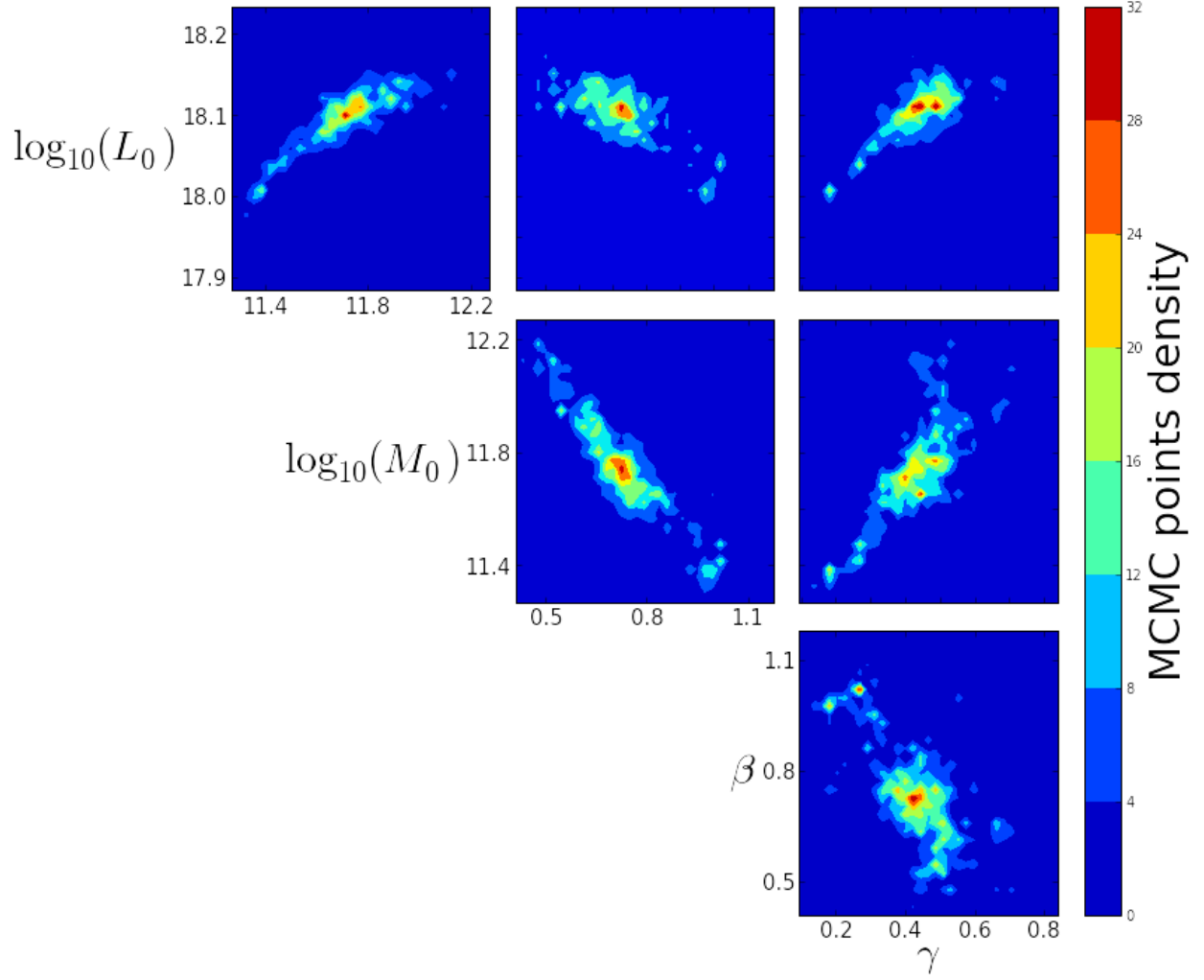
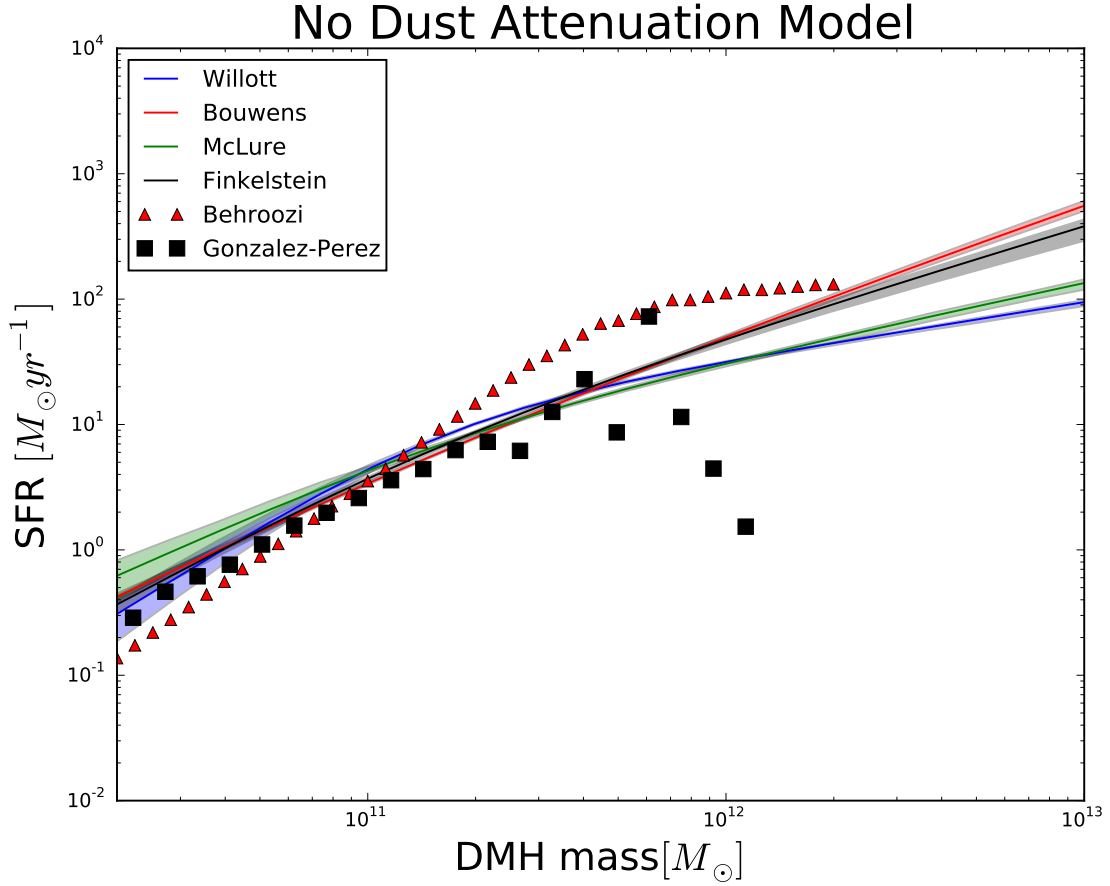Fig. 6.— Covariance of parameters for one small box

Fig. 7.— Star formation rate as function of the dark matter halo mass without dust attenuation. Solid lines represents the mean SFR value over the small boxes within 50% shaded region. Comparison with the GALFORM semi-analitical model (Gonzalez-Perez et al 2014) and a implementation of abundance matching model (Behroozi et al. 2013).
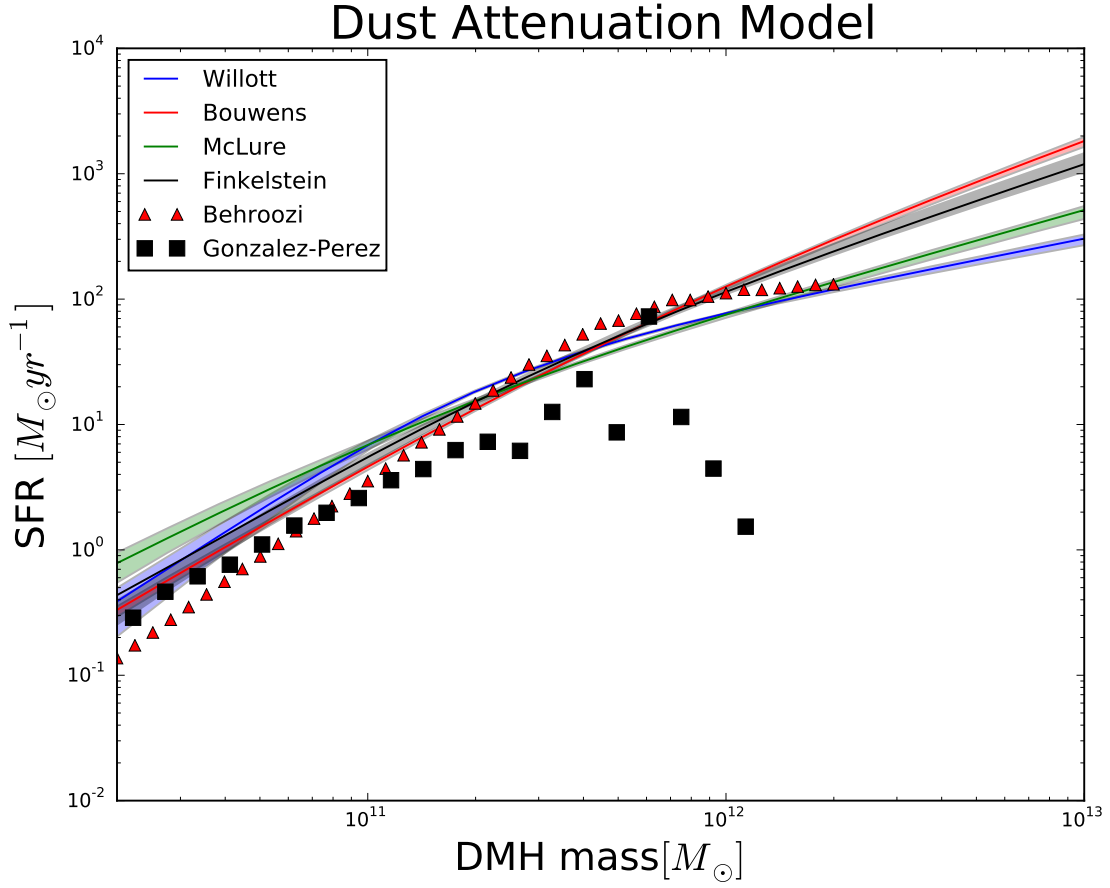
Fig. 8.— Star formation rate as function of the dark matter halo mass with dust attenuation. Solid lines represents the mean SFR value over the small boxes within 50% shaded region. Comparison with the GALFORM semi-analitical model (Gonzalez-Perez et al 2014) and a implementation of abundance matching model (Behroozi et al. 2013).

4. Discussion

REFERENCES

Behroozi, Peter S., Risa H. Wechsler, Charlie Conroy. 2013, ApJ, 770, 57

Bouwens, R. J. et al. 2006, ApJ, 653, 53

Bouwens, R. J. et al. 2012a, ApJ, 752, 5

Bouwens, R. J., G. D. Illingworth, P. A. Oesch, M. Franx, I. Labb, M. Trenti, P. van Dokkum, et al. 2012b. ApJ, 754,83

Bouwens, R. J., G. D. Illingworth, P. A. Oesch, M. Trenti, I. Labbe', L. Bradley, M. Carollo, et al. 2014, arXiv:1403.4295

Colín, Pedro, Anatoly A. Klypin, Andrey V. Kravtsov, and Alexei M. Khokhlov. 1999, ApJ, 523,32

Conroy, Charlie, Risa H. Wechsler, Andrey V. Kravtsov. 2006, ApJ,647,201

Efstathiou, G., Richard S. Ellis, Bruce A. Peterson. 1988, MNRAS, 232,431.

Finkelstein, Steven L., Russell E. Ryan Jr., Casey Papovich, Mark Dickinson, Mimi Song, Rachel Somerville, Henry C. Ferguson, et al. 2014, arXiv:1410.5439

Gonzalez-Perez, V., C. G. Lacey, C. M. Baugh, C. D. P. Lagos, J. Helly, D. J. R. Campbell, and P. D. Mitchell. 2014.MNRAS, 439, 264

Kennicutt, Robert C., Jr. 1998, ARA&A, 36, 189

Kennicutt, Robert C., Jr et al. 2009, ApJ, 703, 4672

Kravtsov, Andrey V., Andreas A. Berlind, Risa H. Wechsler, Anatoly A. Klypin, Stefan Gottlber, Brandon Allgood, Joel R. Primack. 2004, ApJ, 609, 35

Klypin, Anatoly A., Sebastian Trujillo-Gomez, and Joel Primack. 2009, ApJ, 740, 102

Anatoly Klypin, Gustavo Yepes, Stefan Gottlober, Francisco Prada Steffen Hess. 2014, arXiv:'1411.4001

Law, K. et al. 2011, ApJ, 738, 124

Jiang, Linhua et al. 2011, ApJ, 743, 65

Lee, Kyoung-Soo et al. 2009, ApJ, 695, 368

Lundgren, Britt F. et al, 2014, ApJ, 780, 34

Madau, Piero. et al, 1998, ApJ, 498, 106M

McLure, R. J., M. Cirasuolo, J. S. Dunlop, S. Foucaud, O. Almaini. 2009, MNRAS, 395, 2196

Meurer, Gerhardt R., Timothy M. Heckman, Daniela Calzetti. 1999, ApJ, 521, 64

Moster, Benjamin P. et al. 2010, ApJ, 710, 903

Planck Collaboration, P. A. R. Ade, N. Aghanim, C. Armitage-Caplan, M. Arnaud, M. Ashdown, F. Atrio-Barandela, et al. A&A, 571, A16

Prada, Francisco, Anatoly A. Klypin, Antonio J. Cuesta, Juan E. Betancort-Rijo, and Joel Primack. 2012. MNRAS, 423, 3018

Riebe, K. et al. 2013, AN, 334, 691

Schmidt, Maarten. 1968, ApJ151, 393.

Smit, Renske, Rychard J. Bouwens, Marijn Franx, Garth D. Illingworth, Ivo Labb, Pascal A. Oesch, Pieter G. van Dokkum. 2012, ApJ756,14

Steidel, Charles C. et al. 2003, ApJ, 592, 728

Trible, Virginia. 1987, ARA&A, 25, 425

van den Bosh, Frank C. et al. 2003, MNRAS, 40, 771

Willott, Chris J., Ross J. McLure, Pascale Hibon, Richard Bielby, Henry J. McCracken, Jean-Paul Kneib, Olivier Ilbert, David G. Bonfield, Victoria A. Bruce, Matt J. Jarvis. 2013, AJ, 145, 4